Chapter 2
Numerical Solution of Space Fractional Advection–Dispersion Equation and Application

Pramod Kumar Sharma, Muskan Mayank, and Pooja Agarwal

Abstract Generally, advection–dispersion and fractional advection–dispersion equations are used to model the transport of solute tracer in a porous medium. This study describes the numerical solution of both the general advection–dispersion equation and the space fractional advection–dispersion equation. The developed numerical model is used to simulate the observed data of chloride concentration obtained in the laboratory using soil column experiments. Different scenarios were used to estimate the transport parameters to simulate the concentration profiles through experiments.

Abbreviations

ADE	Advection–dispersion equation
FADE	Fractional advection–dispersion equation
sFADE	Spatial fractional advection–dispersion equation
BTC	Breakthrough curve
FEM	Finite element method
D50	Mean size particle
OF	Objective function
NSE	Nash–Sutcliffe efficiency coefficient
RMSE	Root mean square deviation

P. K. Sharma (✉) · P. Agarwal
Department of Civil Engineering, Indian Institute of Technology Roorkee, Roorkee 247667, India
e-mail: pramod.sharma@ce.iitr.ac.in

P. Agarwal
e-mail: pagarwal@ce.iitr.ac.in

M. Mayank
Department of Civil Engineering, National Institute of Technology, Srinagar (Garhwal), Uttarakhand, India
e-mail: muskan.mayank@nituk.ac.in

P. Shukla et al. (eds.), *Environmental Processes and Management*, Water Science and Technology Library 120, https://doi.org/10.1007/978-3-031-20208-7_2

2.1 Introduction

Advection is proportional to mean water velocity. Sternberg (2004) demonstrated that for a macroscopic condition, the experimentally determined dispersion coefficient behaves asymptotically through heterogeneous porous media. It is well understood, however, that this coefficient is spatially dependent and that it is not constant in heterogeneous porous media (Gelhar et al. 1992). Early breakthroughs and long tails characterize breakthrough curves in these cases. This is referred to as non-Fickian phenomenon. These anomalous dispersal characteristics cannot be explained by the traditional advection–dispersion equation (ADE) with constant coefficients. Benson et al. (2001) developed the spatial fractional advection–dispersion equation (sFADE) to address this issue.

Ben-Zvi et al. (2016) proposed a one-dimensional FEM solution by studying intro-differential advection–dispersion equations which have important applications for anomalous transport in highly disordered porous media. The formulation has been used to model the non-Fickian solute transport in porous media. Kundu (2018) studied the concentration distribution in suspension for turbulent flows using the fractional advection–diffusion equation. In addition, Sharma et al. (2020) conducted experiments in soil columns in the laboratory to investigate the non-Fickian behavior of solute transport through both homogeneous and heterogeneous porous media.

In the present study, we briefly discussed the advection–dispersion equation and the space fractional advection–dispersion equation. The sFADE model is then solved using the numerical explicit finite difference method. Chloride concentration profiles were obtained in the laboratory using soil column experiments. To investigate obtained concentration profiles at different lengths in the direction of flow, both the ADE and sFADE models were used. Different scenarios have been used to estimate transport parameters and simulated the concentration profiles.

2.2 Theoretical Concepts

2.2.1 Equations Influencing ADE

For reactive solutes with linear isotherm equilibrium adsorption, the equation can be written as (Bear and Cheng 2010):

$$R\frac{\partial C}{\partial t} + v\frac{\partial C}{\partial x} = D\frac{\partial^2 C}{\partial x^2} \tag{2.1}$$

For nomenclature explanations, refer the list of parameters.

2.2.2 Equations Influencing sFADE

Considering a linear isotherm equilibrium adsorption, the one-dimensional FADE for reactive solute can be expressed (Benson et al., 2000a, 2000b):

$$R\frac{\partial C}{\partial t} + v\frac{\partial C}{\partial x} = \left(\frac{1}{2} + \frac{\beta}{2}\right) D_f \frac{\partial^\alpha C}{\partial x^\alpha} + \left(\frac{1}{2} - \frac{\beta}{2}\right) D \frac{\partial^\alpha C}{\partial (-x)^\alpha} \tag{2.2}$$

For nomenclature explanations, refer the list of parameters.

The transition probability for $-1 \leq \beta \leq 0$ is skewed backward, whereas for $0 \leq \beta \leq 1$, the transition probability is skewed forward. For $\beta = 0$, the above equation can be expressed as:

$$R\frac{\partial C}{\partial t} + v\frac{\partial C}{\partial x} = \left(\frac{1}{2}\right) D_f \frac{\partial^\alpha C}{\partial x^\alpha} + \left(\frac{1}{2}\right) D \frac{\partial^\alpha C}{\partial (-x)^\alpha} \tag{2.3}$$

$$C(x,t) = C_0\left[1 - F_\alpha\left(\frac{x - vt/R}{(\Re t)^{1/\alpha}}\right)\right] \tag{2.4a}$$

where $\Re = |\cos(\pi\alpha/2)| D_f/R$, $F_\alpha(y)$ is the probability function that is symmetric α-stable:

$$F_\alpha(y) = C(\alpha) + \frac{\text{sign}(1-\alpha)}{2} \int_0^1 \exp\left(-y^{\frac{\alpha}{\alpha-1}} U_\alpha(\varphi)\right) \mathrm{d}\varphi \tag{2.4b}$$

where φ is the integration variable, $\text{sign}(1-\alpha)$ is -1, 0 and $+1$ for $\alpha > 1$, $\alpha = 1$ and $\alpha < 1$, respectively, and, $C(\alpha)$ and U_α can be expressed as:

$$C(\alpha) = \begin{cases} 1 & \text{for}\, \alpha > 1 \\ 0.5 & \text{for}\, \alpha < 1 \end{cases} \tag{2.4c}$$

$$U_\alpha(\varphi) = \left(\frac{\sin(\pi\alpha\varphi/2)}{\cos(\pi\varphi/2)}\right)^{\left(\frac{\alpha}{1-\alpha}\right)} \tag{2.4d}$$

2.2.3 sFADE Equations and Its Numerical Solution

Derivation of a numerical scheme to solve sFADE is described in Meerschaert and Tadjeran 2004 and 2006, as:

$$\frac{\partial^\alpha C(x,t)}{\partial x^\alpha} = \lim \operatorname*{Lim}_{M_+ \to \infty} \frac{1}{h_+^\alpha} \sum_{k=0}^{M_+} g_k C(x - kh, t) \tag{2.5a}$$

And,

$$\frac{\partial^\alpha C(x,t)}{\partial (-x)^\alpha} = \lim \operatorname*{Lim}_{M_- \to \infty} \frac{1}{h_+^\alpha} \sum_{k=0}^{M_-} g_k C(x + kh, t) \tag{2.5b}$$

The Grunwald weights g_k are defined as follows:

$$g_0 = 1 \tag{2.6a}$$

$$g_k = (-1)^k \frac{\alpha(\alpha-1)(\alpha-2)\ldots(\alpha-k+1)}{k!} \tag{2.6b}$$

$$\frac{\partial^\alpha C(x_i,t_n)}{\partial x^\alpha} = \frac{1}{h^\alpha} \sum_{k=0}^{M} g_k C(x_i - (k-1)h, t_n) \tag{2.7a}$$

Conversely, the right-sided fractional derivatives with the shifted Grunwald approximation

$$\frac{\partial^\alpha C(x_i,t_n)}{\partial (-x)^\alpha} = \frac{1}{h^\alpha} \sum_{k=0}^{M} g_k C(x_i + (k-1)h, t_n) \tag{2.7b}$$

The Grunwald weights are represented by g_k in these expressions.

$$\frac{C_i^{l+1} - C_i^l}{\Delta t} = -v \frac{C_{i+1}^l - C_{i-1}^l}{2h} + \frac{D_f}{2h^\alpha} \left(\sum_{k=0}^{M} g_k C_{i-k+1}^l + \sum_{k=0}^{M} g_k C_{i+k-1}^l \right) \tag{2.8}$$

In the internal points of the spatial domain, $(i = 1, \ldots, M-1)$, one has

$$C_i^{l+1} = \frac{D_f \Delta t}{2h^\alpha} \sum_{k=0}^{M} g_k C_{i-k+1}^l + \frac{D_f \Delta t}{2h^\alpha} \sum_{k=0}^{M} g_k C_{i+k-1}^l - \frac{v\Delta t}{2h} C_{i-1}^l + \frac{v\Delta t}{2h} C_{i-1}^l + C_i^l \tag{2.9}$$

The stability condition is $\left(\frac{v\Delta t}{h} + \frac{\alpha D_f \Delta t}{h^\alpha} \right) \leq 1$.

2.2.4 Experimental Procedure

On a 300 cm long horizontally placed soil column, a soil column experiment was carried out. Chloride was chosen as a non-reactive tracer for the experiment. The soil column is densely packed with sand of the mean particle size (D50). The value of the cumulative distribution's particle size diameter is at 50%. The calculated value of mean particle size (D50) for fine sand is 0.75 mm, D10 = 0.37 mm, D30 = 0.68 mm, D60 = 0.8 mm, Cc = 1.56 mm, Cu = 2.16. During the solute transport experiment, the soil column was gradually saturated with de-aired tap water from the soil column's inlet. As a result, the soil column's entrapped air was removed. A peristaltic pump was used to inject a common salt (NaCl) solution with an initial solute concentration of C0 = 60 mg/L. The total volumetric water content of the soil media within the column was estimated to be 0.34. The soil media's calculated dry bulk density was found to be 1.71 g/cm^3.

2.2.4.1 Goodness-of-Fit and Estimation of Parameters

The inverse problem method was used to estimate the mathematical model's parameters. An inverse model with the following objective function was created to obtain the parameters (Moradi and Mehdinejadiani 2020).

$$\mathrm{OF} = \frac{1}{N}\sum_{i=1}^{N}\left(C_i^{\mathrm{calc}} - C_i^{\mathrm{obs}}\right)^2 \tag{2.10}$$

The root mean square error, coefficient of determination, and Nash–Sutcliffe efficiency coefficients are all expressed below:

$$R^2 = \left[\frac{\sum_{i=1}^{N}\left(C_i^{\mathrm{obs}} - \overline{C}^{\mathrm{obs}}\right)\left(C_i^{\mathrm{calc}} - \overline{C}_i^{\mathrm{calc}}\right)}{\sqrt{\sum_{i=1}^{N}\left(C_i^{\mathrm{obs}} - \overline{C}^{\mathrm{obs}}\right)^2}\sqrt{\sum_{i=1}^{N}\left(C_i^{\mathrm{calc}} - \overline{C}^{\mathrm{calc}}\right)^2}}\right]^2 \tag{2.11}$$

$$\mathrm{RMSE} = \sqrt{\frac{1}{N}\sum_{i=1}^{N}\left(C_i^{\mathrm{obs}} - C_i^{\mathrm{calc}}\right)^2} \tag{2.12}$$

Nash–Sutcliffe efficiency coefficient (NSE) can be calculated by:

$$\mathrm{NSE} = 1 - \frac{\sum_{i=1}^{N}\left(C_i^{\mathrm{obs}} - C_i^{\mathrm{calc}}\right)^2}{\sum_{i=1}^{N}\left(C_i^{\mathrm{obs}} - \overline{C}^{\mathrm{obs}}\right)^2} \tag{2.13}$$

2.2.5 Results and Discussion

The results have been predicted for three cases. In the first case, we estimated the ADE as well as sFADE transport parameters at various points and used these estimates to simulate the observed chloride concentration profiles. Transport parameters were estimated at a distance of $x = 40$ cm in the second case, while in the third case, we estimated the values of transport parameters for observed breakthrough curves at upstream, i.e., at $x = 300$ cm, and used to simulate observed breakthrough curves at downstream distances.

2.2.5.1 Estimation of Transport Parameters of ADE and sFADE at Various Points

Table 2.1 shows the evaluated values of parameters for ADE along with sFADE, as well as the allied values of and NSE at various points in the flow direction. A constant value of pore velocity ($v = 2.12$ cm/min) was used in this simulation. The estimation of the predicted profile of concentrations at 40 cm using both the ADE and sFADE models is shown in Fig. 2.1a. Similarly, Fig. 2.1a–g shows simulations of observed concentration profiles at different points. These concentration profile simulation results show that the sFADE model outperforms the ADE model. The estimated results show that the coefficient of determination and NSE values for the ADE and sFADE models are nearly identical. The RMSE values, on the other hand, have varied. It demonstrates that the RMSE is lower for simulated results of observed concentration profiles at distances of 40 and 300 cm. Furthermore, for all distances, the estimated values of for the sFADE model are less than 2. This implies that the behavior of solute transport is non-Fickian.

Table 2.1 Estimated parameters for ADE and sFADE at variable distances

Distance (cm)	ADE				sFADE				
	D (cm^2/min)	R^2	RMSE	NSE	D_f cm$^\alpha$/min	α	R^2	RMSE	NSE
40	0.812	0.997	0.0339	0.994	0.982	1.861	0.996	0.030	0.995
80	1.365	0.996	0.0344	0.994	1.656	1.846	0.987	0.050	0.987
120	1.768	0.998	0.0322	0.995	2.012	1.824	0.990	0.045	0.990
160	2.051	0.997	0.0354	0.994	2.134	1.787	0.989	0.049	0.988
200	2.562	0.998	0.0426	0.990	2.765	1.756	0.988	0.050	0.987
250	2.893	0.998	0.0374	0.993	3.050	1.785	0.987	0.052	0.986
300	3.014	0.999	0.0347	0.994	3.126	1.864	0.997	0.025	0.997

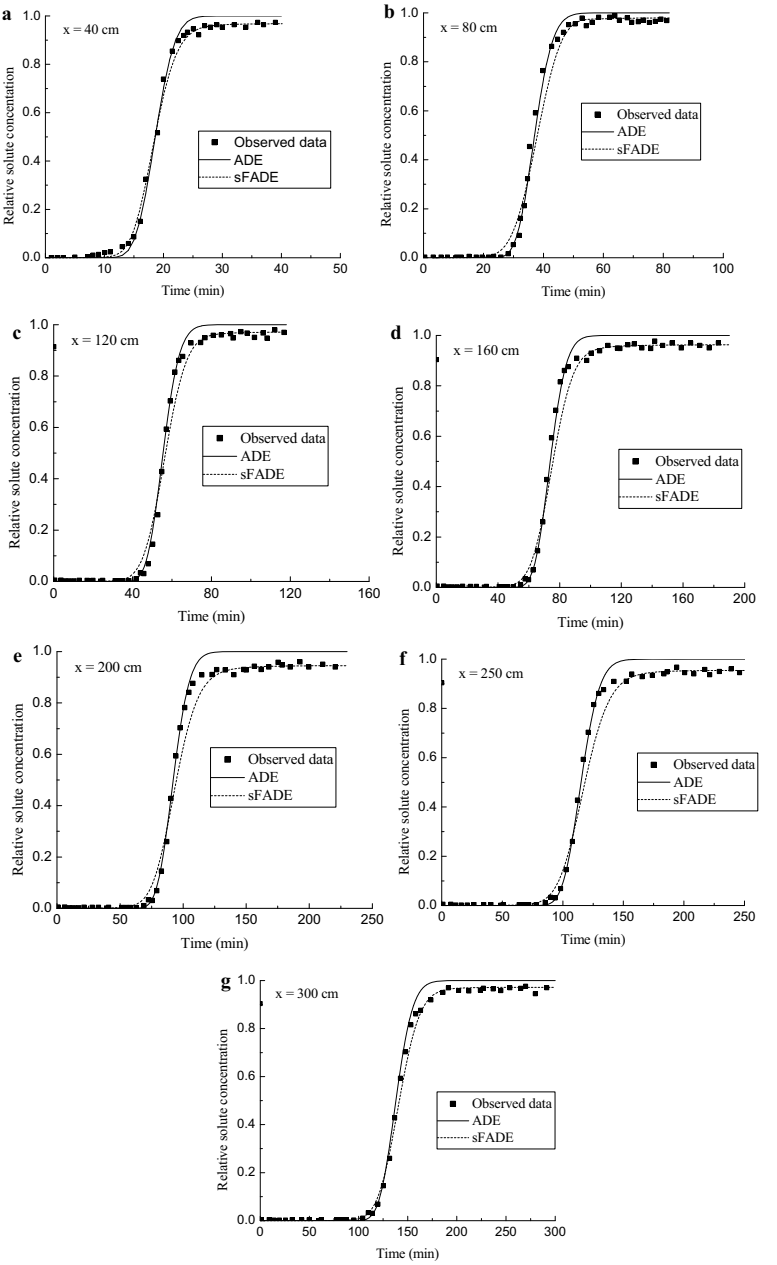

Fig. 2.1 **a** BTCs (at $x = 40$ cm) using ADE and sFADE, **b** BTCs of Cl^- (at $x = 80$ cm) using ADE and sFADE, **c** BTCs of Cl^- (at $x = 120$ cm) using ADE and sFADE, **d** BTCs of Cl^- (at $x = 160$ cm) using ADE and sFADE, **e** BTCs of Cl^- (at $x = 200$ cm) using ADE and sFADE, **f** BTCs of Cl^- (at $x = 250$ cm) using ADE and sFADE, **g** BTCs of Cl^- (at $x = 300$ cm) using ADE and sFADE

Table 2.2 Estimated parameters at 40 cm are used to simulate data at 80, 120, 200, 250 and 300 cms

Distance (cm)	ADE				sFADE				
	D (cm^2/min)	R^2	RMSE	NSE	D_f cm$^\alpha$/min	α	R^2	RMSE	NSE
40	0.812	0.997	0.034	0.994	0.983	1.86	0.996	0.030	0.995
80	0.812	0.995	0.041	0.991	0.983	1.86	0.997	0.027	0.996
120	0.812	0.998	0.040	0.992	0.983	1.86	0.999	0.015	0.999
160	0.812	0.993	0.053	0.986	0.983	1.86	0.995	0.033	0.995
200	0.812	0.991	0.064	0.978	0.983	1.86	0.996	0.036	0.993
250	0.812	0.987	0.069	0.975	0.983	1.86	0.993	0.043	0.990
300	0.812	0.989	0.063	0.980	0.983	1.86	0.995	0.034	0.994

2.2.5.2 Transport Parameters were Estimated at Distance of $x = 40$ cm. Simulation Done at Distances of $x = 80$, 120, 160, 200, 250 and 300 cm

In this case, the observed breakthrough curves at different points upstream in the flow direction were simulated using estimated transport parameters for the observed concentration profile at $x = 40$ cm (Table 2.2). The coefficient of determination and NSE have roughly the same value, as can be seen. The RMSE value, however, is lower in the sFADE model than in the ADE model, as shown in Table 2.2 and Fig. 2.2a–f.

2.2.5.3 Estimation of Transport Parameters for Observed Breakthrough Curves at Upstream ($x = 300$ cm) used for Simulation at Downstream Distances

In this case, the parameter values (i.e., D, D_f and α) are estimated at x = 300 cm in the flow direction and are shown in Table 2.3. These parameters have been used to estimate the obtained concentration profiles at variable points as shown in Fig. 2.3a–f. In this case, the values of the coefficient of determination are greater in the ADE model than in the sFADE model. Furthermore, the RMSE values for the ADE model are lower than those for the FADE model (Table 2.3).

2.2.5.4 Estimation of the Mean Values of Solute Transport Parameters

In this case, mean value of parameters, i.e., D, D_f and α for ADE and sFADE, has been utilized to estimate the obtained concentration profiles at various points as shown in Table 2.4. Simulated concentration profiles employing both ADE and sFADE models are shown in Fig. 2.4a–g. Values of RMSE indicate that the best simulation is obtained from sFADE model at distances of $x = 200$ cm, 250 cm, and 300 cm, respectively. When comparing the ADE model to the sFADE model, the

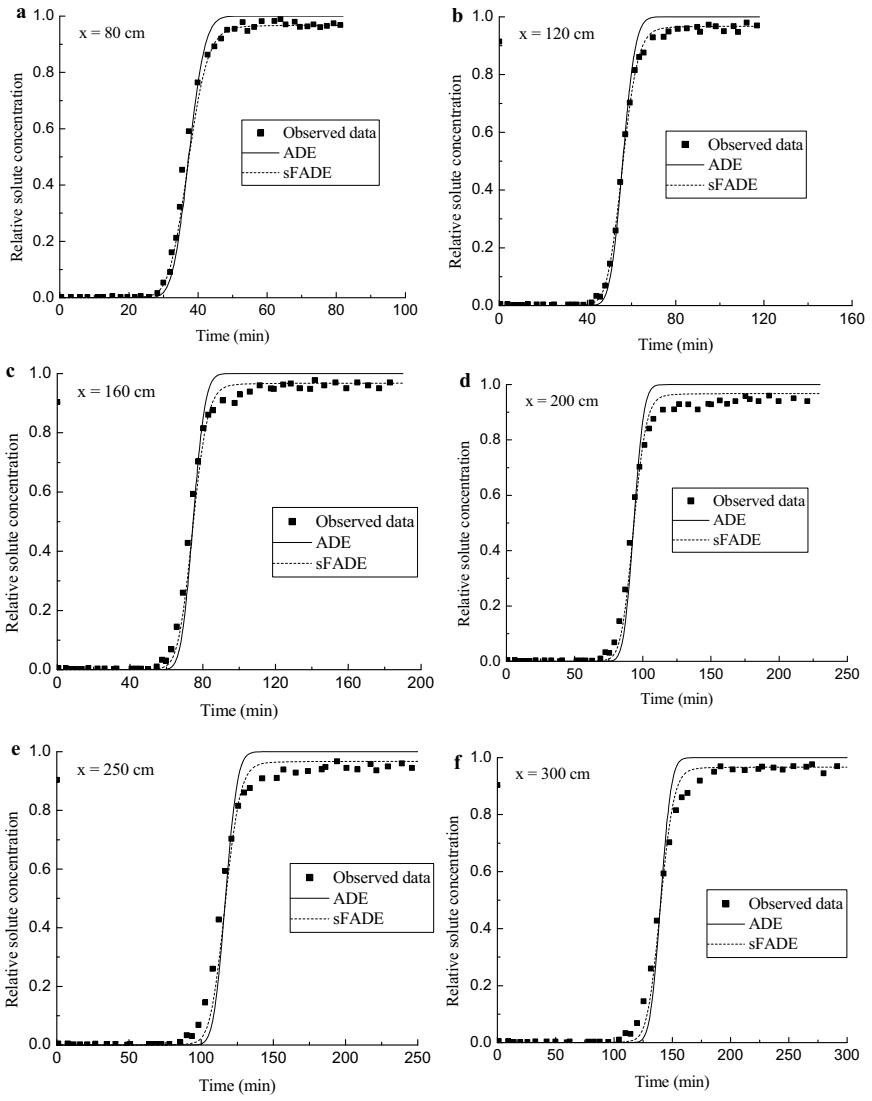

Fig. 2.2 **a** BTCs of Cl^- at $x = 80$ cm using estimated parameters of ADE and sFADE at $x = 40$ cm breakthrough curves, **b** The BTCs of Cl^- at $x = 120$ cm using estimated parameters of ADE and sFADE at $x = 40$ cm breakthrough curves, **c** BTCs of Cl^- at $x = 160$ cm using estimated parameters of ADE and sFADE at $x = 40$ cm breakthrough curves, **d** BTCs of Cl^- at $x = 200$ cm using estimated parameters of ADE and sFADE at $x = 40$ cm breakthrough curves, **e** BTCs of Cl^- at $x = 250$ cm using estimated parameters of ADE and sFADE at $x = 40$ cm breakthrough curves, **f** BTCs of Cl^- at $x = 300$ cm using estimated parameters of ADE and sFADE at $x = 40$ cm breakthrough curves

Table 2.3 Estimated parameters at 300 cm are used to simulate data at 250, 200, 160, 80 and 40 cms

Distance (cm)	ADE				sFADE				
	D (cm^2/min)	R^2	RMSE	NSE	D_f cm$^\alpha$/min	α	R^2	RMSE	NSE
40	3.014	0.976	0.070	0.974	3.126	1.864	0.964	0.095	0.952
80	3.014	0.990	0.047	0.989	3.126	1.864	0.982	0.066	0.978
120	3.014	0.990	0.050	0.987	3.126	1.864	0.984	0.059	0.982
160	3.014	0.995	0.038	0.992	3.126	1.864	0.987	0.052	0.986
200	3.014	0.998	0.043	0.990	3.126	1.864	0.992	0.039	0.992
250	3.014	0.998	0.037	0.993	3.126	1.864	0.993	0.039	0.992
300	3.014	0.999	0.035	0.994	3.126	1.864	0.997	0.025	0.997

RMSE value is lower (at $x = 40$, 80, 120 and 160 cm). This means that the ADE model provides better simulation at a few distances while the sFADE model provides better simulation at other distances.

2.2.5.5 Variation of RMSE and Coefficient of Determination

An attempt has been made to plot the variation of RMSE and coefficient of determination with distances in the flow direction. Four cases are selected; i.e., parameters are estimated at different distances (Case-A), estimated parameters at $x = 40$ cm

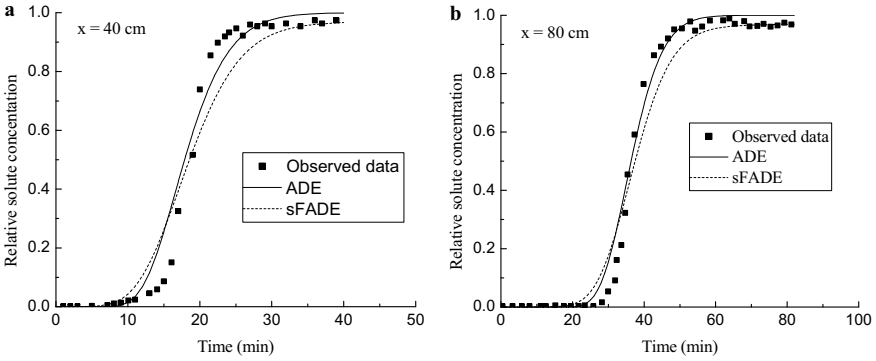

Fig. 2.3 **a** BTCs of Cl^- at $x = 40$ cm using estimated parameters of ADE and sFADE at $x = 300$ cm breakthrough curves, **b** BTCs of Cl^- at $x = 80$ cm using estimated parameters of ADE and sFADE at $x = 300$ cm breakthrough curves, **c** BTCs of Cl^- at $x = 120$ cm using estimated parameters of ADE and sFADE at $x = 300$ cm breakthrough curves, **d** BTCs of Cl^- at $x = 160$ cm using estimated parameters of ADE and sFADE at $x = 300$ cm breakthrough curves, **e** BTCs of Cl^- at $x = 200$ cm using estimated parameters of ADE and sFADE at $x = 300$ cm breakthrough curves, **f** BTCs of Cl^- at $x = 250$ cm using estimated parameters of ADE and sFADE at $x = 300$ cm breakthrough curves

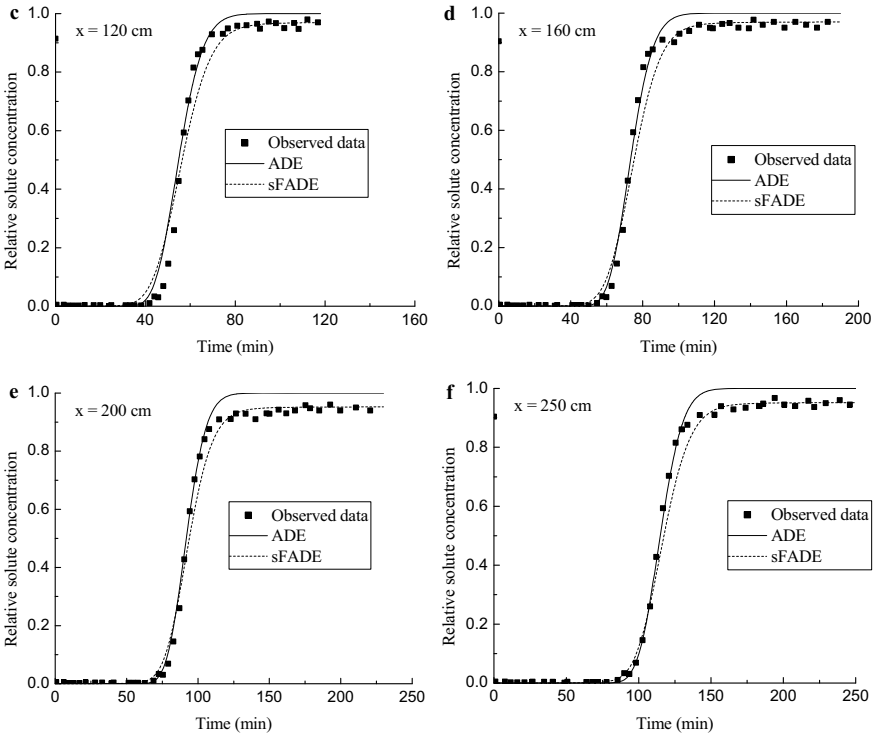

Fig. 2.3 (continued)

Table 2.4 Mean values of parameters are used to simulate data at different distances

Distance (cm)	ADE				sFADE				
	D (cm^2/min)	R^2	RMSE	NSE	D_f cm$^\alpha$/min	α	R^2	RMSE	NSE
40	2.066	0.987	0.051	0.986	2.464	1.818	0.969	0.089	0.958
80	2.066	0.994	0.037	0.993	2.464	1.818	0.984	0.062	0.980
120	2.066	0.996	0.036	0.993	2.464	1.818	0.985	0.057	0.983
160	2.066	0.997	0.036	0.993	2.464	1.818	0.988	0.050	0.988
200	2.066	0.998	0.044	0.990	2.464	1.818	0.991	0.040	0.991
250	2.066	0.997	0.043	0.990	2.464	1.818	0.991	0.043	0.990
300	2.066	0.998	0.039	0.992	2.464	1.818	0.998	0.022	0.998

have been used to determine the obtained concentration profiles at different points (Case-B), estimated parameters at $x = 300$ cm are used to simulate concentration profiles (Case-C), and mean values of parameters are used to simulate concentration profiles at various distances (Case-D). Figures 2.5 and 2.6 indicate the variation of coefficient of determination with distance for ADE as well as sFADE models.

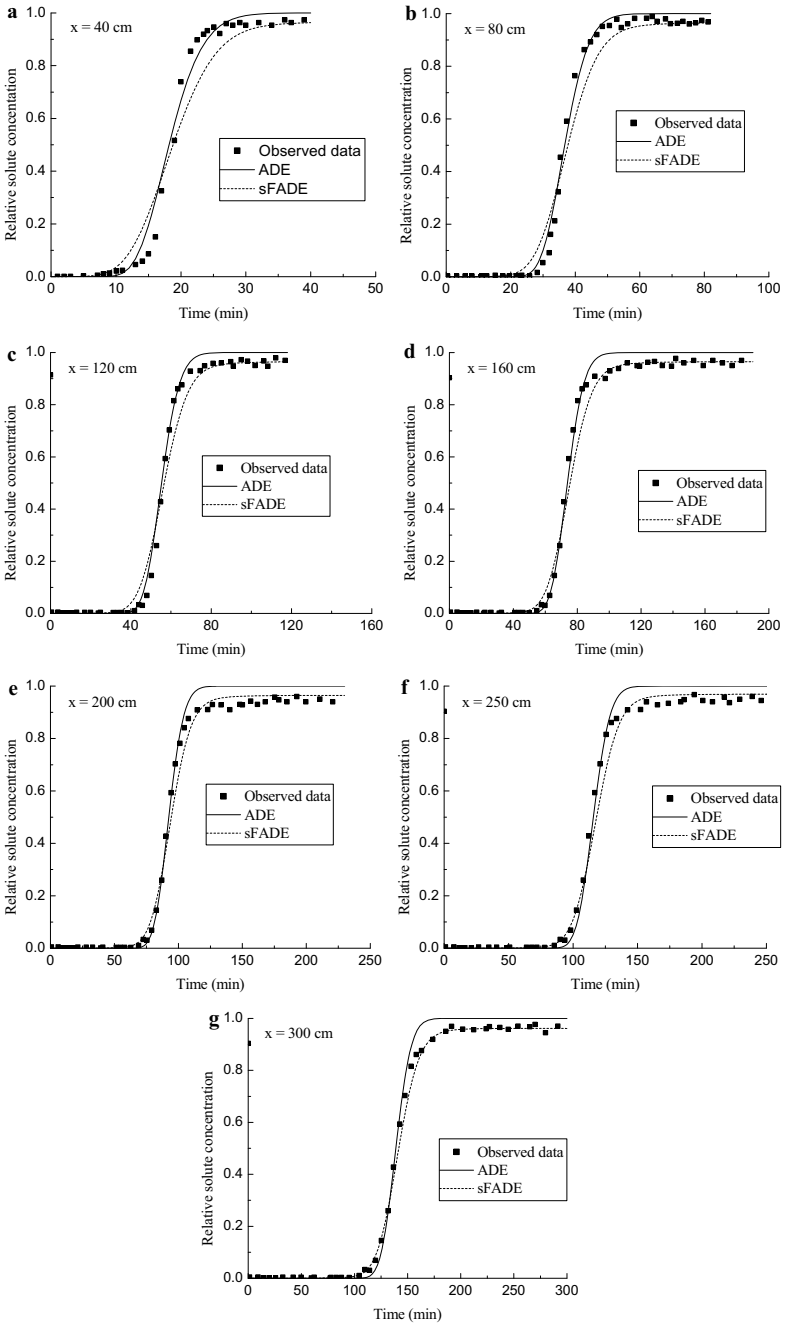
a
x = 40 cm
b
x = 80 cm
c
x = 120 cm
d
x = 160 cm
e
x = 200 cm
f
x = 250 cm
g
x = 300 cm
Observed data
ADE
sFADE
Relative solute concentration
Time (min)

◂**Fig. 2.4** **a** BTCs of Cl^- at $x = 40$ cm using mean value of parameters of ADE and sFADE, **b** BTCs of Chloride at $x = 80$ cm using the mean value of parameters of ADE and sFADE, **c** BTCs of Cl^- at $x = 120$ cm using mean value of parameters of ADE and sFADE, **d** BTCs of Cl^- at $x = 160$ cm using mean value of parameters of ADE and sFADE, **e** BTCs of Cl^- at $x = 200$ cm using mean value of parameters of ADE and sFADE, **f** BTCs of Cl^- at $x = 250$ cm using the mean value of parameters of ADE and sFADE, **g** BTCs of Cl^- at $x = 40$ cm using mean values of parameters of ADE and sFADE

The value of the coefficient of determination remains constant across all cases—A, B, C, and D. Figures 2.7 and 2.8 show the variation of RMSE with distance for various cases for both the ADE and the sFADE models. These findings show that the variation of RMSE at different distances is not uniform for both models.

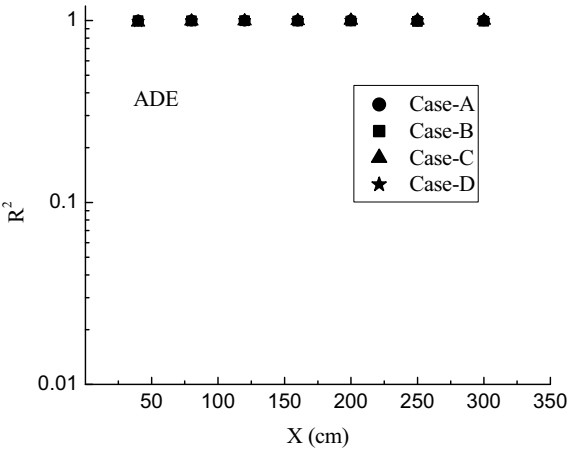

Fig. 2.5 Variation of coefficient of determination with distance in the flow direction for ADE

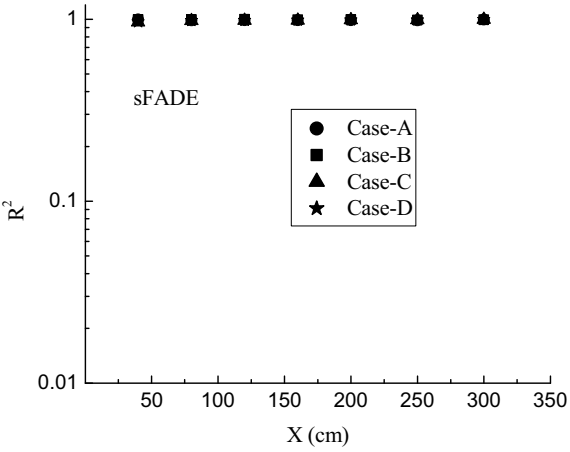

Fig. 2.6 Variation of coefficient of determination with distance in the flow direction for sFADE

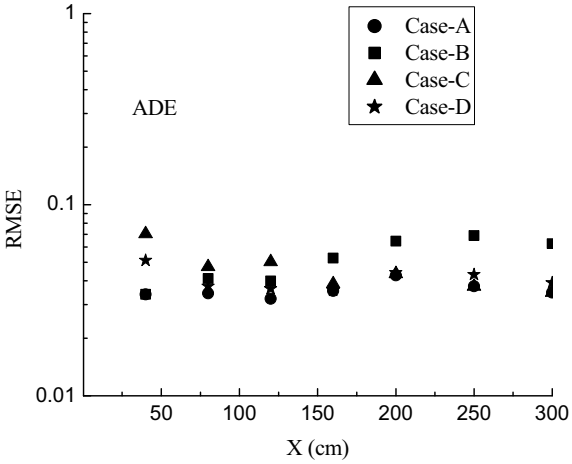

Fig. 2.7 Variation root mean square error (RMSE) with distance in the flow direction for ADE

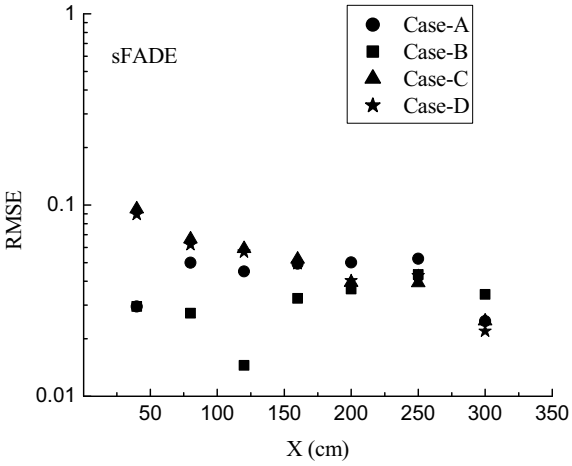

Fig. 2.8 Variation root mean square error (RMSE) with distance in the flow direction for sFADE

2.3 Summary

This study attempted to investigate the performance of the ADE and sFADE models. The solution of the sFADE equation was obtained using an explicit finite difference method. For both the ADE and sFADE models, transport parameters are estimated for various cases. The order of fractional differentiation () in the sFADE model is less than 2. It implies that solute transport is not Fickian in porous media. The determination coefficient and NSE for both the ADE and sFADE models are nearly constant across cases. The RMSE, on the other hand, varies with distance for both models. The RMSE value of the sFADE model is lower when compared to the ADE

model. As a result, the non-Fickian transport model more accurately reproduces observed chloride breakthrough curves through porous media.

References

Bear J, Cheng AHD (2010) Modeling groundwater flow and contaminant transport. vol 23. Springer Science & Business Media

Benson DA, Wheatcraft SW, Meerschaert MM (2000a) The fractional-order governing equation of Lévy motion. Water Resour Res 36(6):1413–1423. https://doi.org/10.1029/2000WR900032

Benson DA, Wheatcraft SW, Meerschaert MM (2000b) Application of a fractional advection-dispersion equation. Water Resour Res 36(6):1403–1412. https://doi.org/10.1029/2000WR900031

Benson DA, Schumer R, Meerschaert MM, Wheatcraft SW (2001). Fractional dispersion, Lévy motion, and the MADE tracer tests. Transp Porous Media 42(1):211–240. https://doi.org/10.1023/A:1006733002131

Ben-Zvi R, Scher H, Jiang S, Berkowitz B (2016) One-dimensional finite element method solution of a class of integro-differential equations: application to non-Fickian transport in disordered media. Transp Porous Media 115(2):239–263

Gelhar LW, Welty C, Rehfeldt KR (1992) A critical review of data on field-scale dispersion in aquifers. Water Resour Res 28(7):1955–1974. https://doi.org/10.1029/92WR00607

Kundu S (2018) Suspension concentration distribution in turbulent flows: an analytical study using fractional advection–diffusion equation. Phys A 506:135–155

Meerschaert MM, Tadjeran C (2004) Finite difference approximations for fractional advection–dispersion flow equations. J Comput Appl Math 172(1):65–77. https://doi.org/10.1016/j.cam.2004.01.033

Meerschaert MM, Tadjeran C (2006) Finite difference approximations for two-sided space-fractional partial differential equations. Appl Numer Math 56(1):80–90. https://doi.org/10.1016/j.apnum.2005.02.008

Moradi G, Mehdinejadiani B (2020) An experimental study on scale dependency of fractional dispersion coefficient. Arab J Geosci 13:409

Sharma PK, Agarwal P, Mehdinejadiani B (2020) Study on non-Fickian behavior for solute transport through porous media. ISH J Hydraul Eng. https://doi.org/10.1080/09715010.2020.1727783

Sternberg SPK (2004) Dispersion measurements in highly heterogeneous laboratory scale porous media. Transp Porous Media 54:107–124. https://doi.org/10.1023/A:1025708313812